ABBA regulates plasma-membrane and actin dynamics to promote radial glia extension

Juha Saarikangas[1], Janne Hakanen[2,3], Pieta K. Mattila[1], Martin Grumet[4], Marjo Salminen[2,3] and Pekka Lappalainen[1,5,*]

Programs in [1]Cellular Biotechnology and [2]Developmental Biology, Institute of Biotechnology, PO Box 56, 00014 University of Helsinki, Finland
[3]Division of Biochemistry, Department of Basic Veterinary Sciences, PO Box 66, 00014 University of Helsinki, Finland
[4]W. M. Keck Center for Collaborative Neuroscience, Rutgers, State University of New Jersey, NJ, USA
[5]Neuroscience Center, PO Box 56, 00014 University of Helsinki, Finland
*Author for correspondence (e-mail: pekka.lappalainen@helsinki.fi)

Accepted 5 February 2008
Journal of Cell Science 121, 1444-1454 Published by The Company of Biologists 2008
doi:10.1242/jcs.027466

Summary

Radial glia play key roles in neuronal migration, axon guidance, and neurogenesis during development of the central nervous system. However, the molecular mechanisms regulating growth and morphology of these extended cells are unknown. We show that ABBA, a novel member of the IRSp53-MIM protein family, is enriched in different types of radial glia. ABBA binds ATP-actin monomers with high affinity and deforms PtdIns(4,5)P_2-rich membranes in vitro through its WH2 and IM domains, respectively. In radial-glia-like C6-R cells, ABBA localises to the interface between the actin cytoskeleton and plasma membrane, and its depletion by RNAi led to defects in lamellipodial dynamics and process extension. Together, this study identifies ABBA as a novel regulator of actin and plasma membrane dynamics in radial glial cells, and provides evidence that membrane binding and deformation activity is critical for the cellular functions of IRSp53-MIM-ABBA family proteins.

Supplementary material available online at
http://jcs.biologists.org/cgi/content/full/121/9/1444/DC1

Key words: ABBA, IMD, Actin, Cytoskeleton, Membrane deformation, Radial glia

Introduction

Development of the central nervous system (CNS) depends on precisely regulated migration of precursor cells into their final locations, where they mature, form appropriate tissue architecture, and send axons to target areas. Different populations of glia are critical for the formation of the CNS. Radial glial cells are derived from the neuroepithelial cells shortly after the onset of neurogenesis and are characterised by a highly polarised morphology. Their somata reside in the ventricular zone whereas the radial processes span the entire thickness of the developing neural tube. Specialised midline radial glia participate in axon guidance and neural tube patterning whereas the processes of more widely distributed radial glia guide newborn neurons towards their final positions. In addition, radial glial cells may act as neuronal progenitors giving rise to most neurons in the cortex as well as in other brain areas (Lemke, 2001; Anthony et al., 2004; Götz and Huttner, 2005). Most radial processes retract later in development, and the cells are transformed into astrocytic glia, which may contribute to the neural stem cell or progenitor population residing in the neurogenic regions of the adult CNS (Doetsch, 2003). However, specific radial glia populations remain in certain parts of the adult the CNS, such as the Bergmann cells in the cerebellum and Müller cells in the retina (Morest and Silver, 2003).

The actin cytoskeleton is a dynamic structure that has a central role in a number of cellular processes involving membrane dynamics and motility. The architecture and dynamics of the actin cytoskeleton are regulated by a plethora of actin-binding proteins, which are controlled by various signalling molecules, including the small GTPases and phosphoinositides (Dent and Gertler, 2003; Di Paolo and De Camilli, 2006; Pollard and Borisy, 2003). The actin cytoskeleton has an essential role in many developmental processes, including the formation of CNS. A number of regulators of actin dynamics have been linked to CNS morphogenesis, axon and dendritic guidance, as well as formation and dynamics of dendritic spines (Lanier et al., 1999; Rakic and Caviness, Jr, 1995; Boquet et al., 2000; Strasser et al., 2004; Tada and Sheng, 2006). In contrast to the rather well-established roles in neurons, regulation of the actin cytoskeleton in glial cells has remained poorly understood, and no glia-specific regulators of the actin cytoskeleton have been reported so far.

A key protein regulating the morphology and density of dentritic spines is the insulin receptor tyrosine kinase substrate p53 (IRSp53) (Choi et al., 2005). IRSp53 is a member of a protein family consisting of five relatively large proteins that share an N-terminal IRSp53 and MIM (missing in metastasis) (IM) domain (Yamagishi et al., 2004). In most cases, these proteins also contain a C-terminal WASP-homology 2 (WH2) domain, a known actin-monomer-binding motif (Lee et al., 2007; Millard et al., 2007). Members of the IM domain protein family appear to be involved in the formation of membrane protrusions, such as filopodia, lamellipodia and plasma membrane ruffles, where they may function downstream of the Rho family of GTPases (Bompard et al., 2005; Mattila et al., 2003; Miki et al., 2000; Millard et al., 2007; Suetsugu et al., 2006b; Disanza et al., 2006). IM domains display remote structural homology to the membrane-deforming Bin-amphiphysin-Rvs (BAR) domains (Itoh et al., 2005; Lee et al., 2007; Millard et al., 2005). However, IM domains were reported to display both actin-filament-bundling (Millard et al., 2005; Yamagishi et al., 2004) and membrane-deforming activities (Mattila et al., 2007; Suetsugu et al., 2006b) and the biological significance(s) of these activities has remained controversial. Furthermore, the exact mechanism by which these proteins promote the formation of plasma membrane protrusions remains to be elucidated.

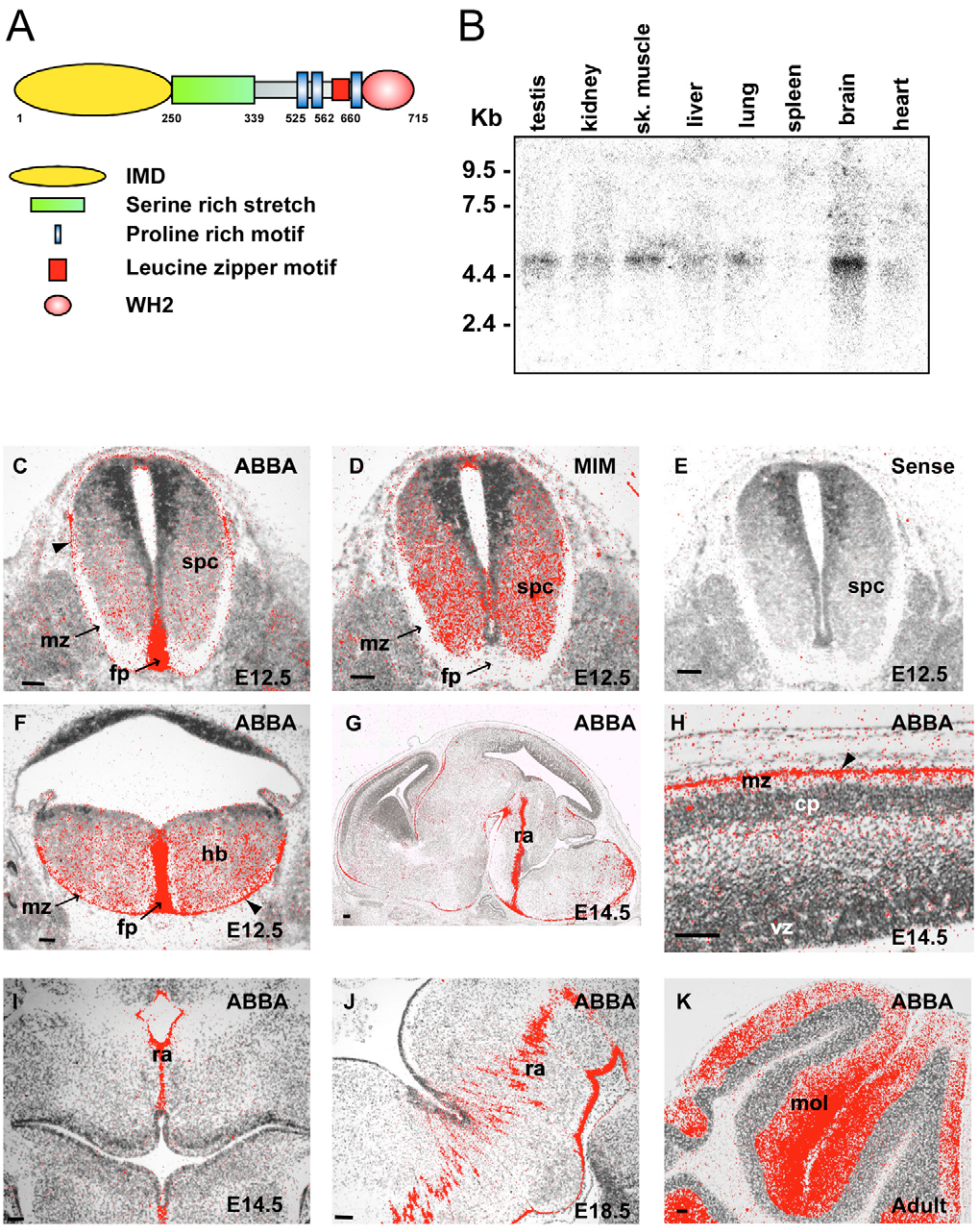

Fig. 1. Domain structure and expression of ABBA. (A) ABBA is composed of an N-terminal IM domain, a serine-rich region, three proline-rich motifs and a C-terminal WH2 domain. (B) Northern blot analysis of ABBA expression in adult mouse tissues shows a single band that was predominant in brain. Each lane contains 2 μg total RNA. RNA in situ hybridisation analysis on sections from mouse embryos at E12.5 (C-F), E14.5 (G-I) and E18.5 (J) and adult cerebellum (K). Probes are indicated in the images. At E12.5 ABBA is strongly expressed in the floorplate of the spinal cord (C) and hindbrain (F), whereas weaker expression is detected in parenchyma and in the outer border of the marginal zone (arrowheads) where radial glia endplates locate. (D) MIM is expressed in spinal cord neurons and its expression is distinct from that of ABBA. (E) No specific signal was obtained with the ABBA sense probe. (G) Sagittal section from E14.5 mouse head where *ABBA* mRNA was detected in the pial surface surrounding the brain and in the midline glial raphe. (H) *ABBA* mRNA was detected in the developing cortex at E14.5 and especially in the outer border of the marginal zone (arrowhead). Cross section at E14.5 (I) and sagittal section at E18.5 (J) show ABBA expression in the brainstem raphe. (K) In the adult brain, the strongest ABBA expression is confined to the molecular layer of the cerebellum. cp, cortical plate; fp, floorplate; hb, hindbrain; mz, marginal zone; ra, glial raphe; spc, spinal cord; vz, ventricular zone. Scale bars: 0.1 mm in C-F, H-K and 0.2 mm in G.

Here we show that a previously uncharacterised member of the IM-domain protein family, ABBA, is specifically expressed in radial glia during CNS development. Biochemical analysis revealed that ABBA induces membrane curvature through its IM domain and interacts with the actin cytoskeleton through its WH2 domain. Interestingly, ABBA localises to the interface between the plasma membrane and the actin cytoskeleton in radial-glia-like C6-R cells, and its depletion results in defects in plasma membrane dynamics and process extension. Together, these studies identify ABBA as the first regulator of cytoskeletal dynamics and cellular morphogenesis in radial glial cells.

Results

ABBA, a novel member of the IM-domain protein family, is specifically expressed in radial glial cells during mouse development

In search of homologues to the IM-domain family proteins MIM and IRSp53 (also known as BAIAP2), we identified a mouse cDNA (*BC060632*) that translates into a 715-residue protein containing a putative N-terminal IM domain (supplementary material Fig. S1A) and a C-terminal WH2 domain. The human homologue of this protein was named ABBA (actin-bundling protein with BAIAP2 homology) (Yamagishi et al., 2004). However, the biochemical and cell biological properties of ABBA have not been characterised. Our database searches revealed that ABBA is highly conserved among vertebrate species ranging from fish to human (supplementary material Fig. S1B). In addition to the IM and WH2 domains, ABBA contains a serine-rich stretch, three proline-rich stretches, and a leucine-zipper motif (Fig. 1A and supplementary material Fig. S1B).

Northern blot analysis revealed that in adult tissues ABBA was predominantly expressed in the brain and moderately in the testis, skeletal muscle and lung (Fig. 1B). Low expression levels were also detected in the kidney, liver and heart. These results were confirmed by RNA in situ hybridisation assays performed on tissue sections (data not shown).

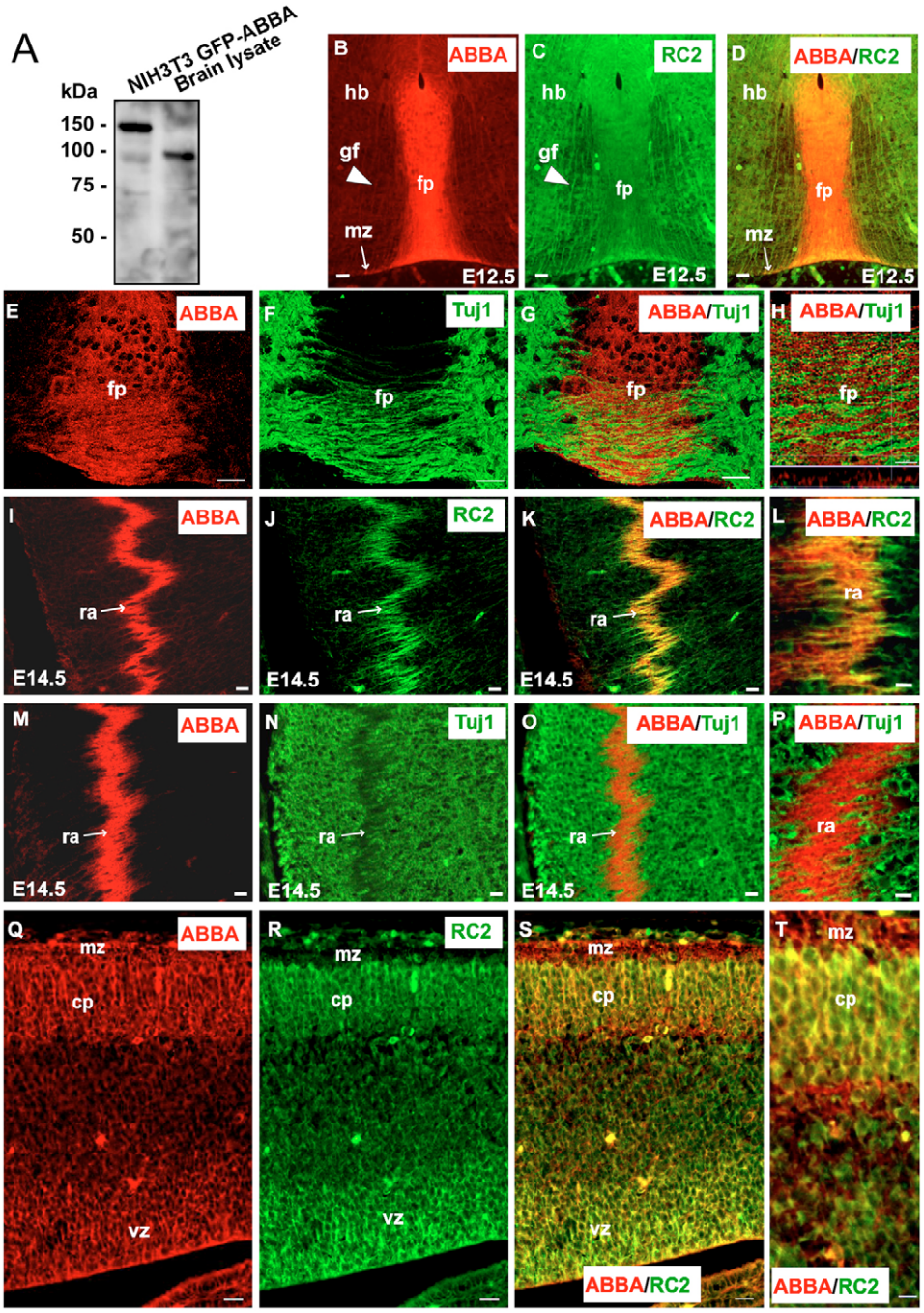

Fig. 2. ABBA is enriched in radial glia. (A) Anti-ABBA antibody recognises a single band from NIH3T3 cell lysate corresponding to the GFP-tagged ABBA, and a lower molecular weight protein from mouse whole brain lysate corresponding to endogenous ABBA. Immunohistochemical detection of ABBA protein (red) on sections from E12.5 (B,E) and E14.5 (I,M,Q) mouse embryonic tissue. Double labelling was performed either with RC2 (C,J,R) or Tuj1 (F,N) (green) and colocalisation with ABBA appears yellow in merged images (D,G,K,O,S) and in corresponding higher magnifications (H,L,P,T). At E12.5, the strongest ABBA expression was detected in the hindbrain floorplate where it colocalised with RC2. ABBA was detected in the radial glia fibers throughout the hindbrain region (arrowhead) and was enriched in the marginal zone where the radial glia end feet are located (arrow) (B-D). No colocalisation was observed with Tuj1, which labelled interneuron axons crossing the ABBA-positive spinal cord floorplate (E-H). At E14.5, ABBA colocalises in glial raphe (arrow) with RC2 (I-L) but not with Tuj1 (M-P). ABBA was detected throughout the developing cortex, where it colocalises in radial glia with RC2 (Q-T). cp, cortical plate; fp, floorplate; hb, hindbrain; mz, marginal zone; ra, glial raphe; gf, glial fiber; vz, ventricular zone. Scale bars: 20 μm in B-G, I-K, M-O, Q-S and 10 μm in H,L,P,T.

To reveal the developmental distribution of ABBA mRNA, we performed RNA in situ hybridisation analyses covering mouse developmental stages E9.5-E18.5. At E9.5-E10.5, *ABBA* mRNA was detected only in the floorplate at the ventral midline of the neural tube from the midbrain until the end of spinal cord (data not shown). The floorplate is a transient structure formed by radially oriented glial cells. At E12.5, the strongest expression was detected in the floorplate area, where *ABBA* mRNA was present especially in the marginal zone containing cellular extensions and only few cell bodies (Fig. 1C). At E12.5, expression became also evident in the outer edge of the marginal zone close to the pial surface, where the radial glial end-feet attach (arrowheads in Fig. 1C,F). Weaker expression was also detected in brain and spinal cord parenchyma (Fig. 1C,F) and in the developing bone and skeletal muscle (data not shown). No signal was detected at any stage with the ABBA sense probe (Fig. 1E and data not shown). The expression of the close homologue MIM was detected in developing neurons and heart (Fig. 1D) (Mattila et al., 2003).

At E14.5, strong expression of *ABBA* was detected in a specific midline glial raphe structure (Fig. 1G,I), as well as in the pial surface surrounding the brain tissue (Fig. 1G), including the cortex (arrowhead in Fig. 1H). Presence of *ABBA* mRNA in the pial surface and in the glial raphe was detected also at E18.5 (Fig. 1J). In the adult brain, the strongest expression of ABBA was detected in the molecular layer of the cerebellum whereas moderate expression was present throughout the brain (Fig. 1K and data not shown). Together,

these analyses suggest that in the developing CNS, ABBA is strongly expressed in different populations of midline radial glial cells and that high levels of *ABBA* mRNA are also present in the pial end-feet of other radial glia.

To confirm that ABBA was indeed expressed in radial glia, we generated a polyclonal antibody against the central region of mouse ABBA protein that is not conserved in other IM-domain proteins. Western blot analysis demonstrated that the antibody detected only a single band of expected mobility from brain lysates and in NIH3T3 cells expressing a GFP-fusion protein of ABBA (Fig. 2A). Furthermore, the antibody did not recognise other IM-domain proteins, IRSp53 and MIM, on a western blot, suggesting that the antibody is specific to ABBA (supplementary material Fig. S2). Immunohistochemical analysis on mouse embryonic tissues at E12.5 revealed that, as with *ABBA* mRNA, the highest level of ABBA protein was present in the floorplate (Fig. 2B). Double labelling with the radial glial marker anti-RC2 showed co-labelling in the floorplate, especially in the cell-body-free zone (Fig. 2D), suggesting that the two proteins colocalised in radial glial cell extensions. Low levels of ABBA protein were detected in the thin radial glial extensions across the hindbrain, together with RC2 (arrowheads in Fig. 2B,C), whereas higher levels were detected in the end-feet areas (arrows in Fig. 2B,D). In the spinal cord, ABBA was detected in floorplate glia that formed intimate contacts with Tuj1-labelled interneuron axons crossing the midline at the cell-body-free zone of the floorplate (Fig. 2E-H). At E14.5, ABBA, together with RC2, was detected in a massive radial glial structure distributed in the midline raphe of the brainstem (Fig. 2I-L). The glial raphe forms a continuous wall-like structure separating the left and right brainstem, and possibly inhibiting growing axons from aberrantly crossing the midline (Mori et al., 1990). Tuj1 labelled adjacent neuronal tissue in the brainstem and no co-labelling with ABBA was detected (Fig. 2M-P), suggesting that ABBA was specifically confined to the radial glia. In the developing cortex, ABBA was detected throughout the tissue colocalising with RC2 in radial glia (Fig. 2Q-T). Similarly to *ABBA* mRNA, ABBA protein staining was strong in the radial glial end-feet area, next to the pial surface. In the adult brain, the highest levels of ABBA were detected in the molecular layer of the cerebellum, both in the Bergmann glia, as well as in the tightly associated Purkinje cell extensions (data not shown).

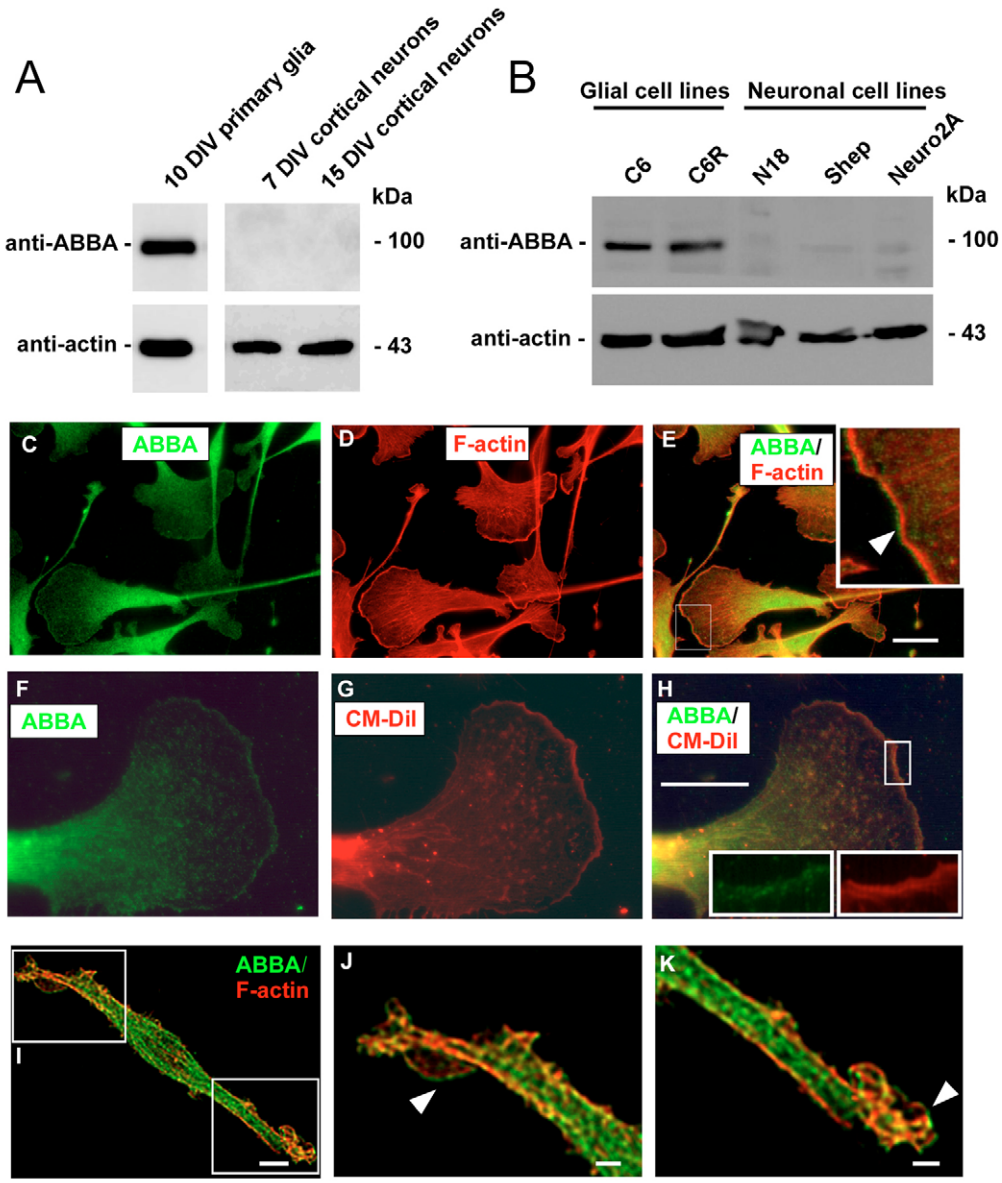

Fig. 3. ABBA is abundantly expressed in glial cell lines where it localises to the interface between plasma membrane and cortical actin cytoskeleton. (A) Western blot analysis demonstrating abundant expression of ABBA in primary glia, whereas cortical neurons derived from E16.5 mouse embryos are negative for ABBA. Anti-actin was used a loading control. (B) ABBA is expressed in glial cell lines (C6 and C6-R), but was not detected in neuronal cell lines (N18, Neuro2A, or Shep). As a loading control, anti-actin antibody was used. (C-E) Immunofluorescence microscopy images from C6-R cells revealed that endogenous ABBA localises in lamellipodia at the leading edge of the cortical actin cytoskeleton (white arrowhead). (F-H) Co-labelling of C6-R cells with ABBA antibody and membrane marker (CM-Dil) demonstrates that ABBA localises to the plasma membrane at the leading edge. (H) Magnified areas show individual channels from the boxed region of the image. (I-K) Three-dimensional confocal microscopy analysis from C6-R cells confirmed the localisation of ABBA to the interface between plasma membrane and the actin cytoskeleton (white arrowheads). ABBA is in green whereas F-actin (panels D,E,I,J,K) and plasma membrane (panels G,H) are in red. Scale bars: 20 μm in C-H; 5 μm in I; 2 μm in J,K.

Western blot analysis using primary glial and neuronal cell extracts derived from E16.5 mouse cortex and cultured in vitro, revealed that ABBA is abundantly expressed in primary glia but not in primary neurons (Fig. 3A). Similarly, cell lysates prepared from glial and neuronal cell lines revealed that ABBA is also specific to glia in cultured cells (Fig. 3B). Together, these studies demonstrated that during CNS development, ABBA is specifically expressed in different types of glia.

Endogenous ABBA localises to the interface between the plasma membrane and the cortical actin cytoskeleton in cultured radial-glial-like cells

To examine the cellular localisation of ABBA we used rat C6-R radial glial cell line. These cells mimic radial glia by expressing radial glial markers, adopting a highly polarised morphology in culture and supporting neuronal migration (Friedlander et al., 1998). In C6-R cells, anti-ABBA antibody revealed strong cytoplasmic staining at the perinuclear area, as previously reported for many other regulators of the actin cytoskeleton. In addition, ABBA displayed specific localisation in the cortical regions at the ends of these highly polarised cells (Fig. 3C). Interestingly, costaining with F-actin revealed that ABBA localised to the front edge of the cortical actin cytoskeleton (Fig. 3E). Co-labelling these cells with membrane marker CM-Dil revealed that ABBA was localised to the plasma membrane (Fig. 3F-H). Confocal microscopy analysis demonstrated the localisation of ABBA to lamellipodial structures and membrane ruffles where ABBA was found at the interface between the cortical actin cytoskeleton and plasma membrane (Fig. 3I-K). Thus, although ABBA localised to the plasma membrane surrounding the cortical actin cytoskeleton, it did not localise to the posterior part of the cortical F-actin network or to actin bundles, as reported for most actin-binding proteins.

ABBA interacts with actin monomers and the small GTPase Rac, but lacks F-actin-bundling activity

To examine whether the conserved WH2 domain of ABBA (supplementary material Fig. S1B) binds actin monomers, we monitored the fluorescence of NBD-labelled actin monomers in the presence of increasing amounts of ABBA. Attempts to express and purify recombinant full-length ABBA were unsuccessful. However, we succeeded in purifying the C-terminal fragment of ABBA (residues 274-715), which contains the WH2 domain, for these assays. Interestingly, $ABBA_{274-715}$ bound ATP-G-actin with ~four

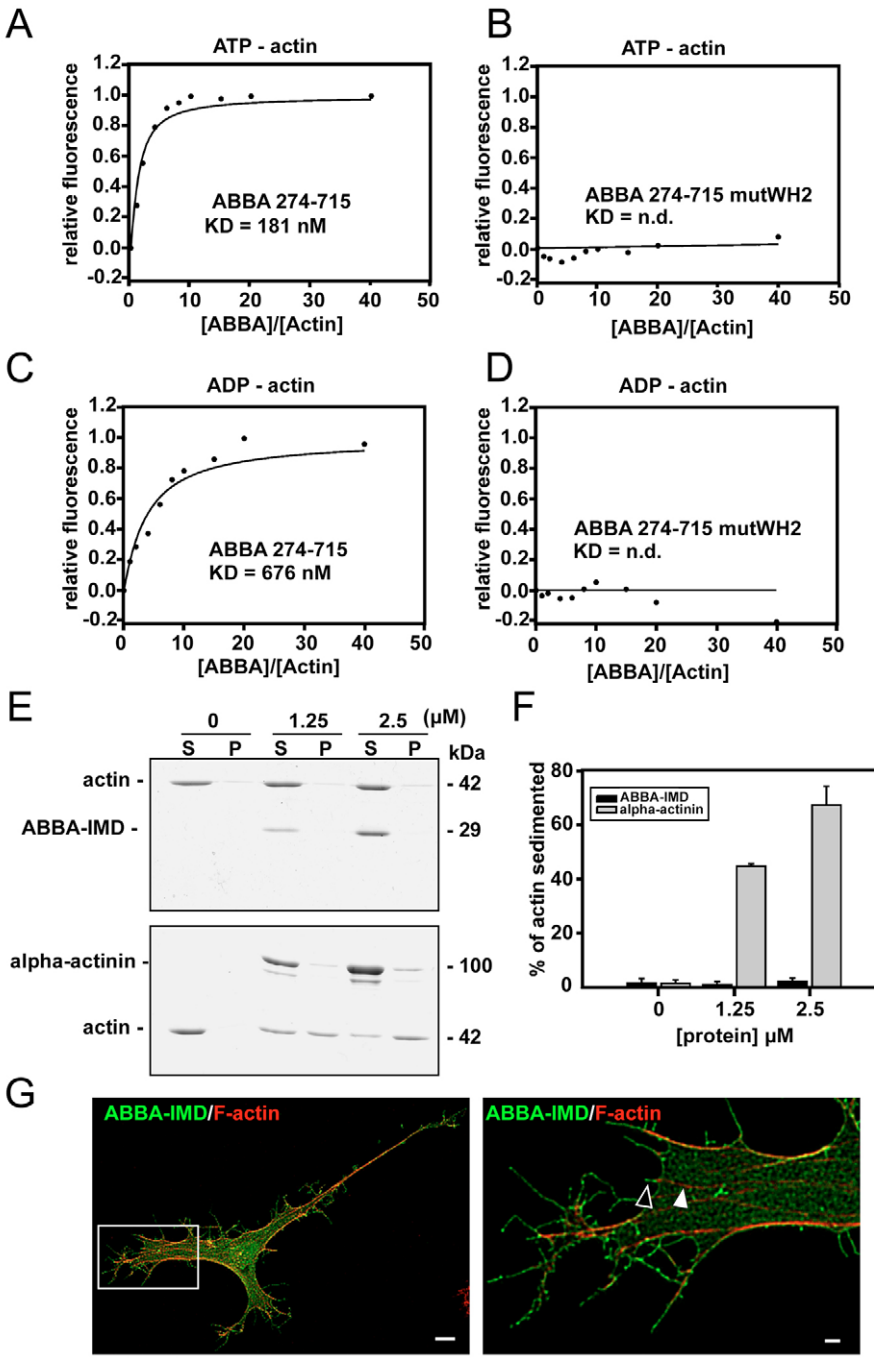

Fig. 4. ABBA binds ATP-G-actin with a high affinity through its C-terminal WH2 domain but does not bundle actin filaments. (A-D) A change in fluorescence of NBD-labelled ATP- and ADP-G-actin was measured over a range of concentrations of $ABBA_{274-715}$. Symbols represent mean data from three experiments and solid lines indicate fitted binding curves with a 1:1 stoichiometry. ABBA interacts with ATP-actin monomers with ~four times higher affinity than ADP-actin monomers. ABBA-mutWH2 did not display detectable binding to G-actin. (E) Low-speed cosedimentation analysis measuring actin-filament-bundling activity of ABBA IM domain (ABBA-IMD). In the presence of α-actinin, majority of actin filaments were in the pellet fraction 'P', demonstrating the actin-filament-bundling or crosslinking activity of the protein. By contrast, under identical conditions, ABBA IMD did not induce detectable actin-filament bundling or crosslinking, and the majority of actin was in the supernatant 'S'. (F) Quantification of bundling activities of ABBA-IMD and α-actinin from two independent experiments. Data are means ± s.e.m. (G) A three-dimensional confocal microscopy analysis from C6-R cells expressing GFP-tagged ABBA-IMD revealed that ABBA-IMD does not localise to peripheral actin bundles (white arrowhead), but instead localises to the plasma membrane surrounding the protruding bundles (black arrowhead). F-actin is red and ABBA-IMD green. Scale bars: 10 μm (left) and 2 μm (magnified region on right).

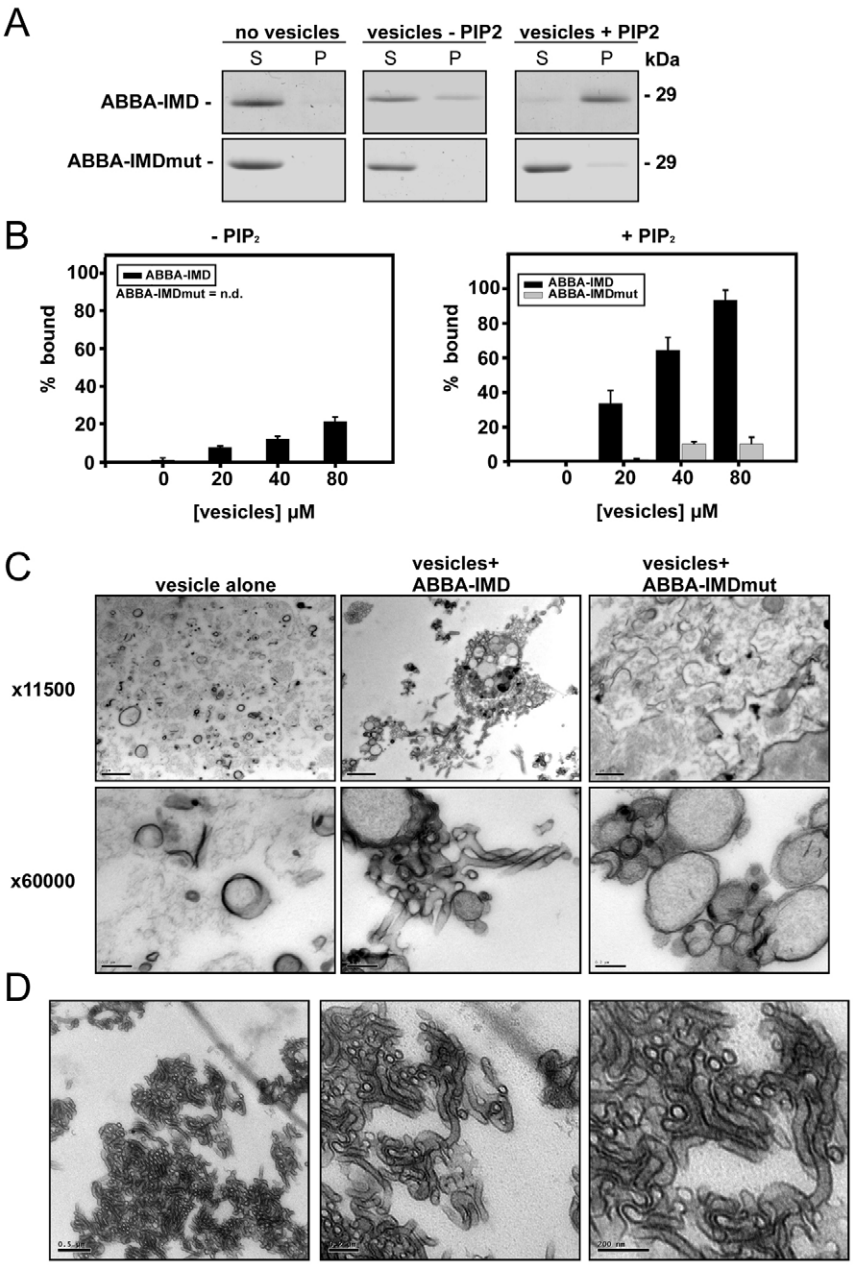

Fig. 5. The ABBA IM domain interacts with PtdIns(4,5)P_2-rich membranes and deforms them into tubular structures. (A) ABBA IM domain (ABBA-IMD) or ABBA-IMDmut were incubated in the absence or presence of vesicles. After centrifugation, equal amounts of supernatant 'S' and pellet 'P' were analysed on SDS-PAGE. ABBA-IMD bound PtdIns(4,5)P_2-containing vesicles with high affinity, whereas ABBA-mutIMD displayed a severe defect in PtdIns(4,5)P_2 binding. (B) Quantification of wild-type ABBA-IMD and ABBA-mutIMD binding to lipid vesicles from three individual experiments. Data are represented as mean ± s.e.m. (C) Electron micrographs of vesicles containing 30% PtdIns(4,5)P_2 mixed with buffer, ABBA-IMD or ABBA-IMDmut. Only wild-type ABBA-IMD induced clustering of vesicles and membrane tubulation. (D) Micrographs of different magnifications showing that ABBA-IMD induced membrane tubules of vesicles containing 5% PtdIns(4,5)P_2. Scale bars: 1 µm in C, upper row; 0.2 µm in C, bottom row; 0.5 µm (left) and 0.2 µm (middle and right) in D.

times higher affinity (K_D=181 nM) (Fig. 4A) than ADP-G-actin (K_D=676 nM) (Fig. 4C). To evaluate the role of the WH2 domain in actin binding, we constructed a mutant protein in which the residues $_{700}$LRR$_{702}$, corresponding to a critical actin-interaction site in other WH2 domains (Chereau et al., 2005), were replaced by alanines (see supplementary material Fig. S1B). This mutant (ABBA$_{274-715}$ mutWH2) did not show detectable binding to ATP- or ADP-G-actin (Fig. 4B,D), confirming that ABBA interacts with actin monomers through its WH2 domain.

ABBA was originally classified as an actin-bundling protein based on sequence similarity to other IM-domain proteins (Yamagishi et al., 2004). Since the actin bundling activity of IM-domain proteins has been controversial (e.g. Millard et al., 2005; Millard et al., 2007; Mattila et al., 2007; Lee et al., 2007), we tested whether the IM domain of ABBA bundles actin filaments. Surprisingly, we could not detect any F-actin-bundling activity with the ABBA IM domain at physiological ionic conditions (100 mM KCl), whereas a well-characterised actin-bundling protein α-actinin displayed strong F-actin bundling activity under identical conditions (Fig. 4E,F). In support to these in vitro results, GFP-tagged ABBA IM domain localised to the plasma membrane (Fig. 4G, black arrowhead), but not to F-actin bundles (Fig. 4G white arrowhead).

Other members of the IM-domain and BAR-protein families were reported to interact with the small GTPases Rac and Cdc42 (Bompard et al., 2005; Krugmann et al., 2001; Miki et al., 2000; Tarricone et al., 2001). GST pull-down assays revealed that ABBA bound both active and inactive forms of Rac, but did not interact with Cdc42 (supplementary material Fig. S2A). Interaction between ABBA and Rac was mediated by the IM domain (supplementary material Fig. S2B). Staining of endogenous ABBA in C6-R cells expressing GFP-tagged active (12V) or inactive (17N) forms of Rac revealed that they are both enriched in the cortical regions of the cell (data not shown).

ABBA IM domain binds and deforms PtdIns(4,5)P_2-rich membranes in vitro and in vivo

IM domains display structural homology to membrane-deforming BAR domains. Recently, IM-domains of MIM and IRSp53 were shown to bind phosphatidylinositol-4,5-bisphosphate [PtdIns(4,5)P_2]-rich membranes and deform them into tubular structures (Mattila et al., 2007; Suetsugu et al., 2006b). To investigate whether ABBA displays similar membrane binding activity, we carried out high-speed co-sedimentation assays using synthetic lipid vesicles. In the absence of PtdIns(4,5)P_2 only ~20% of the ABBA IM domain co-sedimented with vesicles, whereas in the presence of PtdIns(4,5)P_2 ~90% of the ABBA IM domain bound to the vesicles in a concentration-dependent manner (Fig. 5A,B). We also constructed a mutant protein (ABBA-IMDmut) where three lysines corresponding to the critical PtdIns(4,5)P_2-binding residues of the MIM IM domain (Mattila et al., 2007), were replaced with alanines (see supplementary material Fig. S1B). In

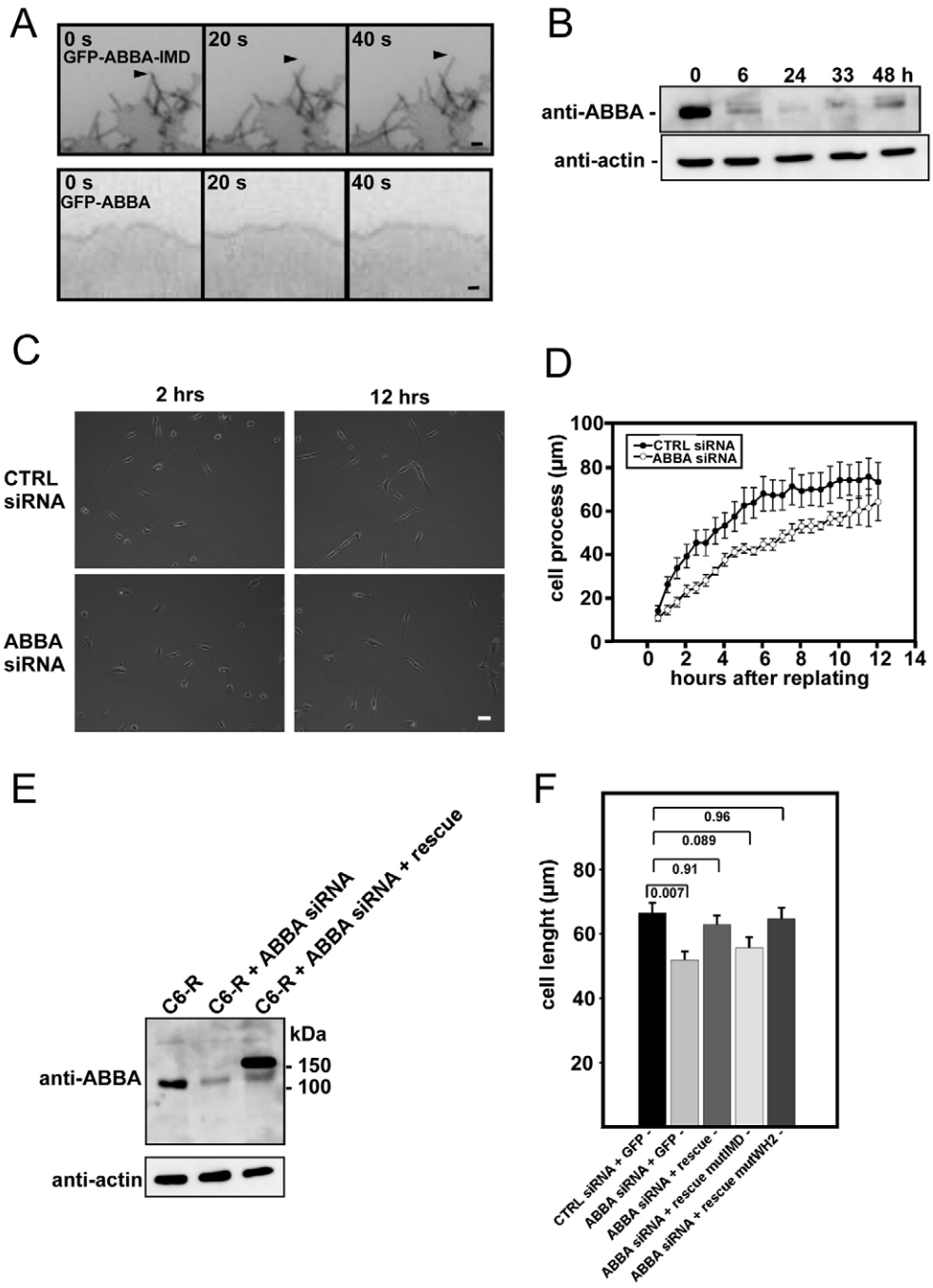

Fig. 6. Depletion of ABBA by siRNA results in glial process extension defects. (A) Time-lapse images from C6-R cells expressing GFP-tagged ABBA IM domain and GFP-tagged full-length protein. Cells expressing the IM domain typically displayed multiple protruding microspikes (black arrowhead), whereas the full-length protein localised to the plasma membrane but did not induce dramatic microspike formation. (B) Western blot analysis demonstrating ABBA protein levels before and after transfection with siRNA oligonucleotides. Anti-actin antibody was used as a loading control. (C) Representative images derived from CellIQ cell imaging platform at 2 and 12 hour time points after replating control siRNA oligonucleotide duplex or with siRNA specific to ABBA-transfected C6-R cells. Scale bar: 5 µm. (D) Graph of mean lengths of C6-R cell processes from six individual wells per group. More than 50 cells were counted in each well. Error bars represent s.e.m. (E) Western blot analysis demonstrating the resistance of ABBA-GFP rescue construct to ABBA siRNA. (F) Quantification of cell lengths from control siRNA or ABBA siRNA-transfected cells that were cotransfected with GFP or siRNA-resistant GFP-ABBA constructs 1.5 hours after replating. Data are represented as mean ± s.e.m. (n=49). Statistical significance was established by one-way ANOVA using Tukey test for comparison.

cosedimentation assays, this mutant displayed a severe defect in PtdIns(4,5)P_2 binding (Fig. 5A,B).

To investigate whether the ABBA IM domain affects conformation of membranes, we mixed lipid vesicles with the ABBA IM domain and analysed the samples using electron microscopy. These experiments revealed that the ABBA IM domain displays strong membrane tubulation activity. In the absence of IM-domains, vesicles were evenly distributed in the sample, whereas the wild-type ABBA IM domain induced clustering and tubulation of the vesicles. Similar clustering was not detected in the presence of the ABBA-IMDmut defective in PtdIns(4,5)P_2 binding (Fig. 5C). IM-domain-induced tubular structures were also observed in vesicles containing a more physiological PtdIns(4,5)P_2 concentration (5%) (Fig. 5D). The tubules induced by the ABBA IM domain were typically very long and displayed a regular diameter of approximately 68±13 nm (mean ± s.d.). A GFP-tagged ABBA IM domain induced massive formation of microspikes in C6-R cells, which is in line with its strong membrane tubulation activity in vitro. These microspikes were highly dynamic and extended several micrometers per minute (Fig. 6A and supplementary material Movie 2).

Since the dynamics of filopodia-like protrusions are considered to be driven by forces created by actin polymerisation, we monitored the growth of ABBA IM-domain-induced microspikes in the presence of the actin polymerisation inhibitor latrunculin A (0.2 µg/µl). This assay revealed a clear reduction in the number of

extending microspikes in the presence of latrunculin A, indicating that the microspike formation depends both on the membrane deformation activity of the IM domain and the polymerisation of actin filaments (supplementary material Fig. S5).

Depletion of ABBA leads to defects in lamellipodial dynamics and impairment of glial process extension

Interestingly, GFP-tagged full-length ABBA did not induce strong microspike formation in C6-R cells compared with cells transfected with an isolated IM domain (Fig. 6A and supplementary material Movies 1 and 2), although it localised to the plasma membrane and membrane ruffles similarly to the endogenous protein (see Fig. 3). Cellular localisation of the endogenous ABBA together with the biochemical data suggested that ABBA might be involved in the regulation of plasma membrane dynamics and cell morphology. To examine this, we silenced ABBA expression by siRNA in C6-R cells. Western blot analysis revealed a dramatic reduction in the levels of ABBA protein at 6-33 hours after siRNA transfection (Fig. 6B). Furthermore, a clear reduction in ABBA protein levels was detected by immunofluorescence in cells transfected with fluorescent ABBA siRNA oligonucleotides compared with neighboring nontransfected cells (data not shown). Depletion of ABBA did not result in gross morphological defects in C6-R cells. Furthermore, no defects in the formation of filopodia induced by activated Cdc42 and Rif constructs were detected in ABBA-knockdown cells (data not shown). To examine the dynamic behaviour of ABBA-knockdown cells, we used CellIQ, an automated cell-imaging platform and monitored the extension of freshly plated C6-R cells. Interestingly, a clear reduction in the velocity of the process extension in ABBA-knockdown cells compared with control cells on both laminin- and collagen-coated surfaces was detected (Fig. 6C,D and data not shown). The maximum velocity of the cell process outgrowth on laminin coated surfaces was ~8 μm/hour in ABBA-knockdown cells compared with ~20 μm/hour in cells transfected with control siRNA duplexes. The difference was further confirmed by transfecting ABBA-knockdown cells simultaneously with siRNA-resistant GFP-rescue or GFP constructs and measuring the total lengths of the cells 1.5 hours after replating (Fig. 6E,F). This analysis also revealed a significant difference between the average lengths of extending control cells and ABBA-knockdown cells ($P<0.01$, Tukey test). Expression of the siRNA-resistant GFP-ABBA construct rescued this defect in ABBA-knockdown cells (Fig. 6F).

To examine the importance of lipid and actin interactions for the function of ABBA in cell morphogenesis, we also carried out siRNA rescue experiments using mutant forms of ABBA. Importantly, expression of an ABBA construct in which the lipid-binding and deformation activities of the IM domain were inactivated by point mutations (described in Fig. 5) did not rescue the knockdown phenotype as efficiently as the construct with an inactivated actin-binding WH2 domain, which rescued the phenotype as efficiently as the wild-type construct (Fig. 6F).

The lack of defects in filopodia formation in ABBA-knockdown cells (data not shown) and the localisation of the endogenous protein to the leading edge of the lamellipodium led us to examine possible defects in lamellipodial dynamics in ABBA-knockdown cells. The behaviour of lamellipodia over time was examined by kymograph analysis, where the slope of a protrusion represents lamellipodial extension velocity (Hinz et al., 1999) (Fig. 7A). Cells were re-plated 24 hours after siRNA transfection and the videos for kymographs were acquired 2-6 hours after re-plating from the most rapidly advancing lamellipodial region (total of 20 cells per group). Although the net velocities of the most rapidly advancing lamellipodial regions over the 10 minute period were similar in wild-type and ABBA knockdown cells (~12 μm/10 min), this analysis revealed a significant decrease in the ruffling frequency and in the speed of individual protrusions in ABBA knockdown cells (Fig. 7B,C).

Discussion

Our findings suggest that ABBA is a multifunctional protein that is utilised for optimisation of plasma membrane dynamics and actin-polymerisation machinery during protrusive events in radial glial cells. This hypothesis is supported by several findings: (1) the WH2 domain of ABBA binds 'polymerisation-competent' ATP-actin monomers with high affinity; (2) the IM domain of ABBA displays strong membrane deformation activity both in vitro and in vivo and thus regulates plasma membrane dynamics during formation of membrane protrusions; (3) endogenous ABBA localises to the interface between the plasma membrane and the actin cytoskeleton in cells; (4) knockdown of ABBA from C6-R cells leads to defects in protrusive events at the lamellipodia of extending radial glial processes – the velocity of individual protrusions is slower and the number of ruffles is decreased in ABBA knockdown cells compared with the control cells.

ABBA is expressed in special subsets of radial glia

During CNS development, ABBA was expressed in specific transient glial structures, whereas no expression was detected in embryonic neurons. The earliest ABBA expression was detected in the midline floorplate, where the first glial cells appear shortly after gastrulation in mammalian embryos. The floorplate is an important signalling center that guides commissural axons across the midline and controls the regional differentiation of neurons along the spinal cord dorso-ventral axis (Patten et al., 2003; Strähle et al., 2004). ABBA was detected later in more widely distributed radial glia throughout the nervous system. A massive radial glial raphe structure becomes apparent in the developing brainstem midline around E13-14.5 and strong expression of ABBA was detected in this structure. The raphe is thought to serve as a control point for axonal extensions through the midline (Mori et al., 1990). In support of the developmental tissue expression data, ABBA protein was found to be abundant in glial cell lines and isolated primary glia, but was undetectable in neuronal cell lines and isolated primary neurons.

Interestingly, RNA in situ hybridisation analysis demonstrated that *ABBA* mRNA was distributed throughout the glial processes and concentrated in the radial glial end-feet indicating that *ABBA* mRNA is transported along the glial processes to the scene of translation. This suggests that a continuous high-level production of ABBA protein in the radial glial extensions may be important during CNS expansion and differentiation. Extension of radial glial end-feet to the pial surface is important for neuronal migration and might have implications for their maturation (Götz et al., 1998; Frotscher et al., 2003; Haubst et al., 2006).

ABBA is a key regulator of glial cell morphology

We found that the extension velocity of ABBA-depleted radial-glia-like C6-R cells was severely diminished compared with that in control cells. The reported growth velocity of radial glial protrusions in vivo is approximately 30 μm/hour (Miyata et al., 2001), which is consistent with the rate of process elongation in wild-type C6-R cells derived from our experiments (~20 μm/hour). However, depletion of ABBA did not affect the net velocity of the most rapidly growing lamellipodial regions, but instead reduced the speed of

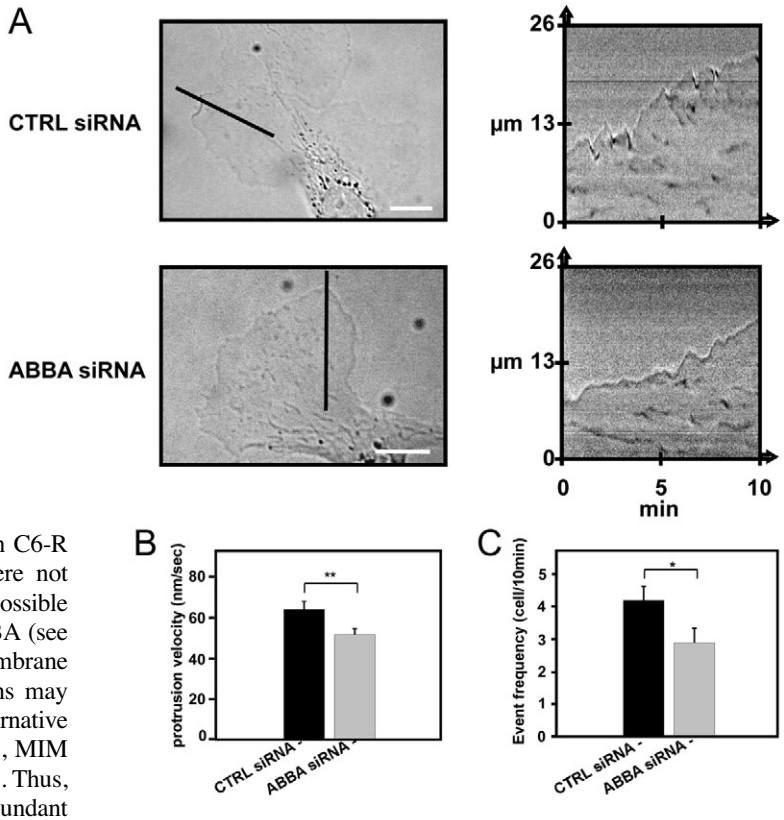

Fig. 7. Depletion of ABBA alters lamellipodial dynamics. (A) Time-lapse movies of C6-R cells transfected with control or ABBA siRNA oligonucleotides were analysed by drawing a one-pixel-wide line across lamellipodium in the direction of protrusion. The kymograph was constructed by copying the image from this line from 200 frames of the movie and pasting along the *x*-axis. Steeper slopes in the kymograph correspond to higher velocity rates in the lamellipodial protrusion. (B) Velocity of individual protrusions was calculated and plotted in the graph. Data were collected from 98 ABBA-knockdown and 105 control protrusion events, error bars represent s.e.m. (C) Individual ruffling events (>0.5 μm) were calculated from kymographs of 20 cells. Data are represented as mean ± s.e.m. $^{**}P<0.02$; $^{*}P<0.05$; Student's *t*-test. Scale bar: 5 μm.

individual plasma membrane protrusions and decreased the ruffling frequency. In line with these data, it was proposed that net cell translocation reflects an integration of cell behaviour over many cycles of protrusion and withdrawal (Bear et al., 2002).

Although depletion of ABBA resulted in clear defects in C6-R cells, plasma membrane dynamics and cell extension were not completely diminished in ABBA-knockdown cells. It is thus possible that the membrane-binding or deformation activity of ABBA (see below) is not absolutely required for formation of membrane protrusions in C6-R cells or that other IM-domain proteins may compensate for the lack of ABBA in C6-R cells. The latter alternative is supported by our RT-PCR analysis showing that IRSp53, MIM and IRTKS are also expressed in C6-R cells (data not shown). Thus, in the future it will be important to study the possible redundant roles of other IM-domain proteins in these and other cells types by simultaneous siRNA knockdown experiments.

Interestingly, a recent microarray study revealed downregulation of *ABBA* mRNA in the brain of *Emx2*-knockout mice (Li et al., 2006). Emx2 is a homeodomain-containing transcription factor that is important in development and patterning of the neocortex (Cecchi, 2002). Importantly, *Emx2*-knockout mouse brains display defects in the morphology of radial glia fibers (Mallamaci et al., 2000). Our data, demonstrating an important role for ABBA in radial glia morphogenesis, suggest that this phenotype may arise from decreased levels of ABBA as well as other cytoskeletal regulators in these mice. In the context of animals, targeted deletion of the *ABBA* gene would be essential to study the role of this protein in radial glia.

Regulation of actin and plasma membrane dynamics by ABBA

ABBA was initially named as 'an actin-bundling protein' based on its sequence similarity to other IM-domain proteins. However, we did not detect any actin-filament-bundling activity of the IM domain of ABBA. Furthermore, neither the GFP-tagged ABBA IM domain nor the endogenous protein localised to actin bundles in vivo as would be expected for an actin-bundling protein. Instead, our analysis revealed that the ABBA IM domain binds PtsIns(4,5)P_2-rich membranes with high affinity and generates membrane curvature similarly to that recently reported for the IM-domain proteins IRSp53 and MIM (Suetsugu et al., 2006b; Mattila et al., 2007). However, from the present EM data, the direction of the membrane deformation cannot be concluded, and this would require extensive electron tomography analysis of the of the membrane tubules induced by the ABBA IM domain. Expression of the GFP-tagged ABBA IM domain in cells induced a massive quantity of filopodia-like membrane protrusions. The extension rate of these protrusions was significantly reduced but not completely abolished upon treatment of the cells with latrunculin A, suggesting that an intact actin cytoskeleton plays an important, but not an essential role in the ABBA IM-domain-induced microspike formation.

Importantly, subcellular localisation of endogenous protein together with siRNA studies suggest that, at least in C6-R cells, ABBA does not promote filopodia formation, but is instead involved in controlling lamellipodial dynamics. Supporting this view, ABBA binds directly to Rac, a well-characterised regulator of lamellipodia dynamics. It is thus likely that interactions with other protein(s) at the leading edge of extending radial glial cells activate ABBA to promote controlled dynamics of lamellipodial protrusions. Further studies will be required to identify these putative binding partners of ABBA.

Previous studies demonstrated that a homologue of ABBA, IRSp53, regulates ruffle formation in fibroblasts and spine formation in neurons (Choi et al., 2005; Suetsugu et al., 2006a). However, the possible physiological role of membrane deformation activity of the IRSp53-MIM family proteins has not been reported and the exact mechanism(s) by which these proteins contribute to cell morphogenesis is unknown. Our RNAi and rescue analyses demonstrate that ABBA regulates plasma membrane dynamics in C6-R cells, and suggest that its membrane-binding or deformation activity is necessary for the efficient formation of cell extensions. Similarly, IRSp53 was recently shown to promote lamellipodia formation and leading-edge extension in cultured animal cells (Suetsugu et al., 2006a). The critical role of membrane-binding or deformation activity for the function of IRSp53-MIM-ABBA family proteins is also supported by our recent studies demonstrating that microspike formation as a result of overexpression of MIM in COS-7 cells is dependent on the intact IM domain (Mattila et al., submitted). However, it still remains to be determined whether IRSp53-MIM family proteins regulate plasma membrane dynamics

by directly deforming the protruding membranes or whether the IM domain functions as a membrane-curvature sensor that localises IRSp53-MIM-ABBA, together with associated proteins, to the correct sites at the plasma membrane.

In addition to plasma membrane, ABBA also binds actin monomers, similarly to its close relative MIM. Importantly, our analysis revealed that ABBA binds ATP-actin monomers with significantly higher affinity than ADP-actin monomers, suggesting that it may promote the addition of actin monomers to the barbed ends of filaments, in a similar manner to other WH2-domain proteins, such as ciboulot and WASP (Hertzog et al., 2004; Dayel and Mullins, 2004). In addition, the WH2 domain of ABBA may interact dynamically with polymerising filament barbed ends, attaching them to plasma membrane by a similar mechanism to that reported recently for N-WASP (Co et al., 2007). However, our RNAi-rescue experiments suggest that, in contrast to membrane-binding or deformation activity, actin-monomer binding through the WH2 domain is not essential for the function of ABBA in C6-R cells. In this context, it is also important to note that the actin-binding WH2 domain is not present in all IM-domain proteins (Lee et al., 2007; Millard et al., 2007). Thus, actin-monomer binding through the WH2 domain may link IM-domain proteins more efficiently to the cytoskeleton during the formation of membrane protrusions.

In conclusion, this study identified ABBA as a protein that couples plasma membrane deformation to the actin cytoskeleton. Therefore, our study provides support to previous hypotheses and theoretical models suggesting that actin dynamics must be linked to direct membrane deformation to efficiently alter the morphology of the plasma membrane during formation of protrusions (Dawson et al., 2006; Veksler and Gov, 2007; Takenawa and Suetsugu, 2007). To our knowledge, ABBA is also the first regulator of actin dynamics and cell morphology that is strongly enriched in radial glia. In the future, it will be important to elucidate how the activity and localisation of ABBA are regulated by various signalling pathways to promote the precisely controlled extension of radial glial processes.

Materials and Methods

Plasmid construction

A DNA fragment corresponding to full-length mouse ABBA cDNA was amplified by PCR from mouse embryo (10-12 days) PCR-ready cDNA (Ambion). This fragment was cloned into pGFP-N1 (Clontech Laboratories) vector. A fragment corresponding to the ABBA IM domain (amino acids 1-249) was subcloned into pGFP-N1, pHAT1 (Peränen et al., 1996) and pBSIIKS vectors. ABBA C-terminal fragments corresponding to residues 274-715 and 274-683 were cloned into the pHAT1 vector. Site-directed mutagenesis was performed as described (Hotulainen and Lappalainen, 2006).

Protein expression and purification

All ABBA constructs were expressed as His-tag fusion proteins in *E. coli* BL21 (DE3) cells. Proteins were enriched with Ni-NTA Superflow beads (Sigma-Aldrich) and further purified through a Superdex-75 HiLoad gel filtration column (GE Healthcare). Human skeletal muscle α-actinin 2 and the small GTPases Rac and Cdc42 were expressed and purified as described (Mattila et al., 2007). Actin was prepared from rabbit skeletal muscle as previously described (Pardee and Spudich, 1982).

Antibody production

A rabbit was immunised with purified recombinant mouse $ABBA_{274-683}$ protein fragment and the serum affinity-purified using this protein fragment immobilised to CNBr-activated Sepharose 4B beads (Pharmacia).

Northern blotting, in situ hybridisations and immunohistochemistry

Northern blotting and in situ hybridisations were carried out as described (Mattila et al., 2003) by using a mouse $ABBA_{1290-1927}$ cDNA probe and [^{35}S]UTP-labelled riboprobes prepared from the linearised pBSIIKS-$ABBA_{1-747}$ plasmid, respectively. For northern blots, the probe was hybridised to commercial mouse multiple tissue filter according to the manufacturer's instructions (Clontech). Immunohistochemistry was performed with anti-ABBA (1:1000), anti-RC2 (1:500; Developmental Studies Hybridoma Bank) and/or anti-Tuj1 (Neuronal Class III β-tubulin; 1:500; BAbCO) primary antibodies overnight at 4°C. Secondary antibodies were goat-anti-mouse IgM Alexa Fluor 488 or goat-anti-rabbit IgG Alexa Fluor 594 (Molecular Probes). Sections were mounted with Vectashield (Vector) and photographed with an Olympus DP70 CCD-camera attached to an Olympus AX70 microscope. Confocal imaging was performed as described (Mattila et al., 2007).

Cell culture and immunofluorescence

The primary neurons and glia were obtained from day 16 embryos. Primary glia and C6-R and NIH3T3 cells were maintained in Dulbecco's modified Eagle's medium supplemented with 10% fetal bovine serum (Hyclone), 2 mM penicillin, streptomycin and L-glutamine (Sigma-Aldrich). Cortical neurons were grown on coverslips coated with poly-DL-ornithine at a density of 0.2×10^6 cells/coverslip in Neurobasal medium supplemented with B27 (Gibco, Life Technologies). Transfections of GFP constructs were carried out using FuGENE 6 transfection reagent (Roche). For immunofluorescence analysis, C6-R cells were plated on coverslips precoated with 25 μg/ml laminin. Immunofluorescence labelling was performed as described previously (Vartiainen et al., 2000) with the following reagent dilutions: Alexa Fluor 568 phalloidin (Molecular Probes), 1:200 and anti-ABBA, 1:50. For membrane staining, C6-R cells were incubated with 2 μM Cell tracker CM-Dil (Molecular Probes) for 5 minutes at 37°C, and then for additional 15 minutes at 4°C after which the medium was changed. Latrunculin A treatment, microscopy, image acquirement and processing were performed as described (Hotulainen and Lappalainen, 2006; Mattila et al., 2007).

Actin assays

The binding of wild-type $ABBA_{274-715}$ and $ABBA_{274-715}$-mutWH2 protein fragments to NBD-labelled actin was carried out as described (Bertling et al., 2007). In the actin-bundling assay, samples were sedimented at 17,000 ***g*** for 30 minutes and the assay was otherwise carried out as described (Mattila et al., 2003).

Lipid assays

Lipid preparations and co-sedimentation assays were performed as previously described (Mattila et al., 2007). For electron microscopy, vesicles (167 μM) containing 0%, 5% or 30% PtdIns(4,5)P_2 were mixed with 22 μM ABBA-IMD dimer in 100 mM HEPES pH 7.5; 100 mM NaCl. Reactions were carried out, fixed, embedded, stained and visualised as described previously (Mattila et al., 2007).

GST pull-down assay

A 60 mm dish of ABBA-GFP transfected HeLa cells was lysed in 100 mM NaCl, 20 mM Tris-HCl, pH 7.5, 0.5 mM PMSF + protease inhibitor cocktail (Roche). 150 μg cleared lysates was incubated for 60 minutes at 4°C with 20 μg recombinant GST or GST-GTPases immobilised on glutathione-agarose beads (Pharmacia). Beads were washed three times with lysis buffer and subjected to western blotting with anti-ABBA antibody. Direct binding of the ABBA IM-domain to the GTPases was analysed as previously described (Mattila et al., 2007).

siRNA treatment and western blotting

For the siRNA treatments, 2 μg preannealed Alexa Fluor 488-labelled ABBA siRNA (target sequence 5′-AAGGACCATGCGAAAGAGTAT-3′) or control siRNA [inverted GL2 sequence targeted to luciferase gene (Elbashir et al., 2001)] were transfected into C6-R cells on six-well plates using the GeneSilencer siRNA transfection reagent (Gene Therapy Systems). For rescue experiments, silent mutations were introduced into the target sequence of GFP-ABBA (5′-AAaGACC-AcGCaAAAGAGTAT-3′) constructs using PCR mutagenesis. Western blotting was performed as described (Hotulainen and Lappalainen, 2006) with the following antibody dilutions: anti-ABBA, 1:500; anti-actin (AC-15; Sigma-Aldrich), 1:10,000.

Cell-spreading assays

ABBA-depleted C6-R cells were replated 24 hours after transfection into 24-well plates precoated with laminin (25 μg/ml). Plates were incubated in CellIQ cell culturing platform (Chip-Man Technologies) and imaged every 30 minutes for 12 hours. For each well, six image fields were collected. For data analysis, RAMON (rapid automated measurement of neurites) software was used. For rescue experiments, cells were transfected with siRNA oligos (0 hour) and GFP-expression constructs (6 hours) resistant to the siRNA oligos, replated on glass coverslips precoated with laminin (28.5 hours), fixed (30 hours) and stained with Alexa Fluor 568-labelled phalloidin. Fifteen cells were imaged per group from more than three independent experiments and the total lengths of the cells in longitudinal direction were measured using ImagePro software (Media Cybernetics).

Kymography and cell tracking

C6-R cells were re-plated 24 hours after siRNA transfection on 25 μg/ml laminin-coated glass-bottomed dishes. Time-lapse images were acquired every 3 seconds for 10 minutes with an inverted microscope (IX70; Olympus) equipped with a Polychrome IV monochromator (TILL photonics) and Uapo 40×/1.35 (water) objective. Kymographs were generated along a 1-pixel-wide line that was drawn by hand perpendicularly to the edge of a protruding cell and constructed using IMAGEJ software (http://rsb.info.nih.gov/ij). Fluctuations <0.5 μm (4 pixels) in magnitude were neglected. Calculation of protrusion velocities was carried out as previously

described (Hinz et al., 1999). Quantification of ruffle frequency was done by calculating the amount of retraction events/cell over 10-minute observation periods.

We thank J. Jäntti, J. Partanen, and J. Peränen for critical reading of the manuscript; M. Bovellan and R. Savolainen for technical assistance; M. Bespalov, P. Hotulainen, M. Palviainen, C. Rivera and M. Vartiainen for reagents and R. Hotulainen for statistical advice. The anti-RC2 developed by M. Yamamoto was obtained from the Developmental Studies Hybridoma Bank developed under the auspices of the NICHD and maintained by The University of Iowa, Department of Biological Sciences. This study was supported by the Research Programme on Neuroscience (NEURO) of Academy of Finland. J.S. was supported by a fellowship from Helsinki Graduate School in Biotechnology and Molecular Biology, J.H. by a fellowship from the Finnish Cultural Foundation and P.K.M. by Alfred Kordelin foundation.

References

Anthony, T. E., Klein, C., Fishell, G. and Heintz, N. (2004). Radial glia serve as neuronal progenitors in all regions of the central nervous system. *Neuron* **6**, 881-890.

Bear, J. E., Svitkina, T. M., Krause, M., Schafer, D. A., Loureiro, J. J., Strasser, G. A., Maly, I. V., Chaga, O. Y., Cooper, J. A., Borisy, G. G. et al. (2002). Antagonism between Ena/VASP proteins and actin filament capping regulates fibroblast motility. *Cell* **4**, 509-521.

Bertling, E., Quintero-Monzon, O., Mattila, P. K., Goode, B. L. and Lappalainen, P. (2007). Mechanism and biological role of profilin-Srv2/CAP interaction. *J. Cell Sci.* **7**, 1225-1234.

Bompard, G., Sharp, S. J., Freiss, G. and Machesky, L. M. (2005). Involvement of Rac in actin cytoskeleton rearrangements induced by MIM-B. *J. Cell Sci.* **22**, 5393-5403.

Boquet, I., Boujemaa, R., Carlier, M. F. and Preat, T. (2000). Ciboulot regulates actin assembly during Drosophila brain metamorphosis. *Cell* **6**, 797-808.

Cecchi, C. (2002). Emx2: a gene responsible for cortical development, regionalization and area specification. *Gene* **1-2**, 1-9.

Chereau, D., Kerff, F., Graceffa, P., Grabarek, Z., Langsetmo, K. and Dominguez, R. (2005). Actin-bound structures of Wiskott-Aldrich syndrome protein (WASP)-homology domain 2 and the implications for filament assebly. *Proc. Natl. Acad. Sci. USA* **46**, 16644-16649.

Choi, J., Ko, J., Racz, B., Burette, A., Lee, J. R., Kim, S., Na, M., Lee, H. W., Kim, K., Weinberg, R. J. et al. (2005). Regulation of dendritic spine morphogenesis by insulin receptor substrate 53, a downstream effector of Rac1 and Cdc42 small GTPases. *J. Neurosci.* **4**, 869-879.

Co, C., Wong, D. T., Gierke, S., Chang, V. and Taunton, J. (2007). Mechanism of actin network attachment to moving membranes: barbed end capture by N-WASP WH2 domains. *Cell* **5**, 901-913.

Dawson, J. C., Legg, J. A. and Machesky, L. M. (2006). Bar domain proteins: a role in tubulation, scission and actin assembly in clathrin-mediated endocytosis. *Trends Cell Biol.* **10**, 493-498.

Dayel, M. J. and Mullins, R. D. (2004). Activation of Arp2/3 complex: addition of the first subunit of the new filament by a WASP protein triggers rapid ATP hydrolysis on Arp2. *PLoS Biol.* **4**, E91.

Dent, E. W. and Gertler, F. B. (2003). Cytoskeletal dynamics and transport in growth cone motility and axon guidance. *Neuron* **2**, 209-227.

Di Paolo, G. and De Camilli, P. (2006). Phosphoinositides in cell regulation and membrane dynamics. *Nature* **443**, 651-657.

Disanza, A., Mantoani, S., Hertzog, M., Gerboth, S., Frittoli, E., Steffen, A., Berhoerster, K., Kreienkamp, H. J., Milanesi, F., Di Fiore, P. P. et al. (2006). Regulation of cell shape by Cdc42 is mediated by the synergic actin-bundling activity of the Eps8-IRSp53 complex. *Nat. Cell Biol.* **12**, 1337-1347.

Doetsch, F. (2003). The glial identity of neural stem cells. *Nat. Neurosci.* **11**, 1127-1134.

Elbashir, S. M., Harborth, J., Lendeckel, W., Yalcin, A., Weber, K. and Tuschl, T. (2001). Duplexes of 21-nucleotide RNAs mediate RNA interference in cultured mammalian cells. *Nature* **441**, 494-498.

Friedlander, D. R., Brittis, P. A., Sakurai, T., Shif, B., Wirchansky, W., Fishell, G. and Grumet, M. (1998). Generation of a radial-like glial cell line. *J. Neurobiol.* **2**, 291-304.

Frotscher, M., Haas, C. A. and Forster, E. (2003). Reelin controls granule cell migration in the dentate gyrus by acting on the radial glial scaffold. *Cereb. Cortex* **6**, 634-640.

Götz, M. and Huttner, W. B. (2005). The cell biology of neurogenesis. *Nat. Rev. Mol. Cell Biol.* **10**, 777-788.

Götz, M., Stoykova, A. and Gruss, P. (1998). Pax6 controls radial glia differentiation in the cerebral cortex. *Neuron* **5**, 1031-1044.

Haubst, N., Georges-Labouesse, E., De Arcangelis, A., Mayer, U. and Gotz, M. (2006). Basement membrane attachment is dispensable for radial glial cell fate and for proliferation, but affects positioning of neuronal subtypes. *Development* **16**, 3245-3254.

Hertzog, M., van Heijenoort, C., Didry, D., Gaudier, M., Coutant, J., Gigant, B., Didelot, G., Preat, T., Knossow, M., Guittet, E. et al. (2004). The beta-thymosin/WH2 domain; structural basis for the switch from inhibition to promotion of actin assembly. *Cell* **5**, 611-623.

Hinz, B., Alt, W., Johnen, C., Herzog, V. and Kaiser, H. W. (1999). Quantifying lamella dynamics of cultured cells by SACED, a new computer-assisted motion analysis. *Exp. Cell Res.* **1**, 234-243.

Hotulainen, P. and Lappalainen, P. (2006). Stress fibers are generated by two distinct actin assembly mechanisms in motile cells. *J. Cell Biol.* **3**, 383-394.

Itoh, T., Erdmann, K. S., Roux, A., Habermann, B., Werner, H. and De Camilli, P. (2005). Dynamin and the actin cytoskeleton cooperatively regulate plasma membrane invagination by BAR and F-BAR proteins. *Dev. Cell* **6**, 791-804.

Krugmann, S., Jordens, I., Gevaert, K., Driessens, M., Vandekerckhove, J. and Hall, A. (2001). Cdc42 induces filopodia by promoting the formation of an IRSp53:Mena complex. *Curr. Biol.* **21**, 1645-1655.

Lanier, L. M., Gates, M. A., Witke, W., Menzies, A. S., Wehman, A. M., Macklis, J. D., Kwiatkowski, D., Soriano, P. and Gertler, F. B. (1999). Mena is required for neurulation and commissure formation. *Neuron* **2**, 313-325.

Lee, S. H., Kerff, F., Chereau, D., Ferron, F., Klug, A. and Dominguez, R. (2007). Structural basis for the actin-binding function of missing-in-metastasis. *Structure* **2**, 145-155.

Lemke, G. (2001). Glial control of neuronal development. *Annu. Rev. Neurosci.* **24**, 87-105.

Li, H., Bishop, K. M. and O'Leary, D. D. (2006). Potential target genes of EMX2 include Odz/Ten-M and other gene families with implications for cortical patterning. *Mol. Cell. Neurosci.* **2**, 136-149.

Mallamaci, A., Mercurio, S., Muzio, L., Cecchi, C., Pardini, C. L., Gruss, P. and Boncinelli, E. (2000). The lack of Emx2 causes impairment of Reelin signaling and defects of neuronal migration in the developing cerebral cortex. *J. Neurosci.* **3**, 1109-1118.

Mattila, P. K., Salminen, M., Yamashiro, T. and Lappalainen, P. (2003). Mouse MIM, a tissue-specific regulator of cytoskeletal dynamics, interacts with ATP-actin monomers through its C-terminal WH2 domain. *J. Biol. Chem.* **10**, 8452-8459.

Mattila, P. K., Pykalainen, A., Saarikangas, J., Paavilainen, V. O., Vihinen, H., Jokitalo, E. and Lappalainen, P. (2007). Missing-in-metastasis and IRSp53 deform PIP2-rich membranes by an inverse BAR domain-like mechanism. *J. Cell Biol.* **7**, 953-964.

Miki, H., Yamaguchi, H., Suetsugu, S. and Takenawa, T. (2000). IRSp53 is an essential intermediate between Rac and WAVE in the regulation of membrane ruffling. *Nature* **408**, 732-735.

Millard, T. H., Bompard, G., Heung, M. Y., Dafforn, T. R., Scott, D. J., Machesky, L. M. and Futterer, K. (2005). Structural basis of filopodia formation induced by the IRSp53/MIM homology domain of human IRSp53. *EMBO J.* **2**, 240-250.

Millard, T. H., Dawson, J. and Machesky, L. M. (2007). Characterisation of IRTKS, a novel IRSp53/MIM family actin regulator with distinct filament bundling properties. *J. Cell Sci.* **9**, 1663-1672.

Miyata, T., Kawaguchi, A., Okano, H. and Ogawa, M. (2001). Asymmetric inheritance of radial glial fibers by cortical neurons. *Neuron* **5**, 727-741.

Morest, D. K. and Silver, J. (2003). Precursors of neurons, neuroglia, and ependymal cells in the CNS: what are they? Where are they from? How do they get where they are going? *Glia* **1**, 6-18.

Mori, K., Ikeda, J. and Hayaishi, O. (1990). Monoclonal antibody R2D5 reveals midsagittal radial glial system in postnatally developing and adult brainstem. *Proc. Natl. Acad. Sci. USA* **14**, 5489-5493.

Pardee, J. D. and Spudich, J. A. (1982). Purification of muscle actin. *Meth. Enzymol.* **85**, 164-181.

Patten, I., Kulesa, P., Shen, M. M., Fraser, S. and Placzek, M. (2003). Distinct modes of floor plate induction in the chick embryo. *Development* **20**, 4809-4821.

Peränen, J., Rikkonen, M., Hyvönen, M. and Kääriäinen, L. (1996). T7 vectors with modified T7lac promoter for expression of proteins in Escherichia coli. *Anal. Biochem.* **2**, 371-373.

Pollard, T. D. and Borisy, G. G. (2003). Cellular motility driven by assembly and disassembly of actin filaments. *Cell* **4**, 453-465.

Rakic, P. and Caviness, V. S., Jr (1995). Cortical development: view from neurological mutants two decades later. *Neuron* **6**, 1101-1104.

Strähle, U., Lam, C. S., Ertzer, R. and Rastegar, S. (2004). Vertebrate floor-plate specification: variations on common themes. *Trends Genet.* **3**, 155-162.

Strasser, G. A., Rahim, N. A., VanderWaal, K. E., Gertler, F. B. and Lanier, L. M. (2004). Arp2/3 is a negative regulator of growth cone translocation. *Neuron* **1**, 81-94.

Suetsugu, S., Kurisu, S., Oikawa, T., Yamazaki, D., Oda, A. and Takenawa, T. (2006a). Optimization of WAVE2 complex-induced actin polymerization by membrane-bound IRSp53, PIP(3), and Rac. *J. Cell Biol.* **4**, 571-585.

Suetsugu, S., Murayama, K., Sakamoto, A., Hanawa-Suetsugu, K., Seto, A., Oikawa, T., Mishima, C., Shirouzu, M., Takenawa, T. and Yokoyama, S. (2006b). The RAC binding domain/IRSp53-MIM homology domain of IRSp53 induces RAC-dependent membrane deformation. *J. Biol. Chem.* **46**, 35347-35358.

Tada, T. and Sheng, M. (2006). Molecular mechanisms of dendritic spine morphogenesis. *Curr. Opin. Neurobiol.* **1**, 95-101.

Takenawa, T. and Suetsugu, S. (2007). The WASP-WAVE protein network: connecting the membrane to the cytoskeleton. *Nat. Rev. Mol. Cell Biol.* **1**, 37-48.

Tarricone, C., Xiao, B., Justin, N., Walker, P. A., Rittinger, K., Gamblin, S. J. and Smerdon, S. J. (2001). The structural basis of Arfaptin-mediated cross-talk between Rac and Arf signalling pathways. *Nature* **411**, 215-219.

Vartiainen, M., Ojala, P. J., Auvinen, P., Peranen, J. and Lappalainen, P. (2000). Mouse A6/twinfilin is an actin monomer-binding protein that localizes to the regions of rapid actin dynamics. *Mol. Cell. Biol.* **5**, 1772-1783.

Veksler, A. and Gov, N. S. (2007). Phase transitions of the coupled membrane- cytoskeleton modify cellular shape. *Biophys. J.* **93**, 3798-3810.

Yamagishi, A., Masuda, M., Ohki, T., Onishi, H. and Mochizuki, N. (2004). A novel actin bundling/filopodium-forming domain conserved in insulin receptor tyrosine kinase substrate p53 and missing in metastasis protein. *J. Biol. Chem.* **15**, 14929-14936.

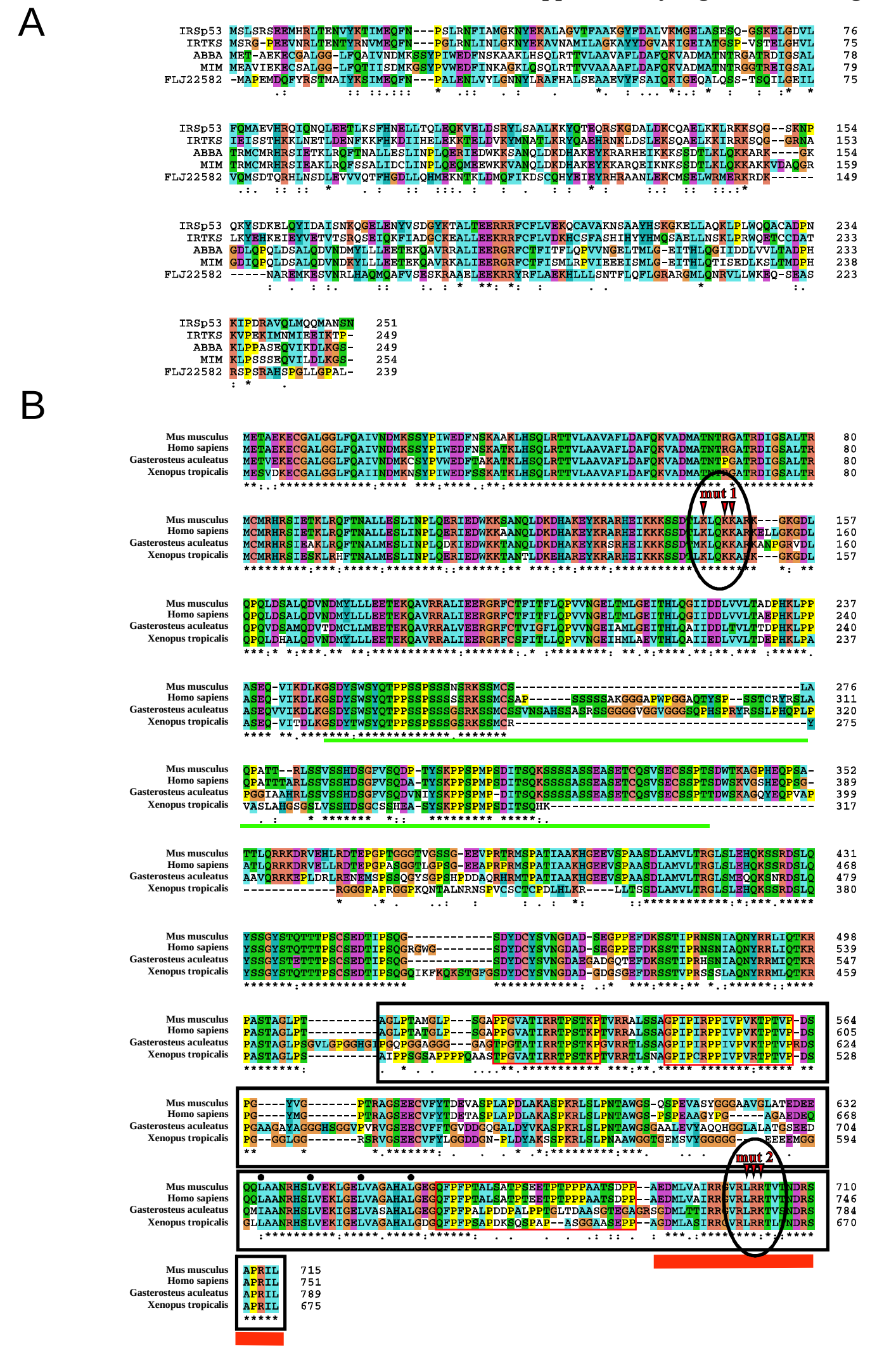
A
IRSp53
IRTKS
ABBA
MIM
FLJ22582
B
Mus musculus
Homo sapiens
Gasterosteus aculeatus
Xenopus tropicalis
mut 1
mut 2

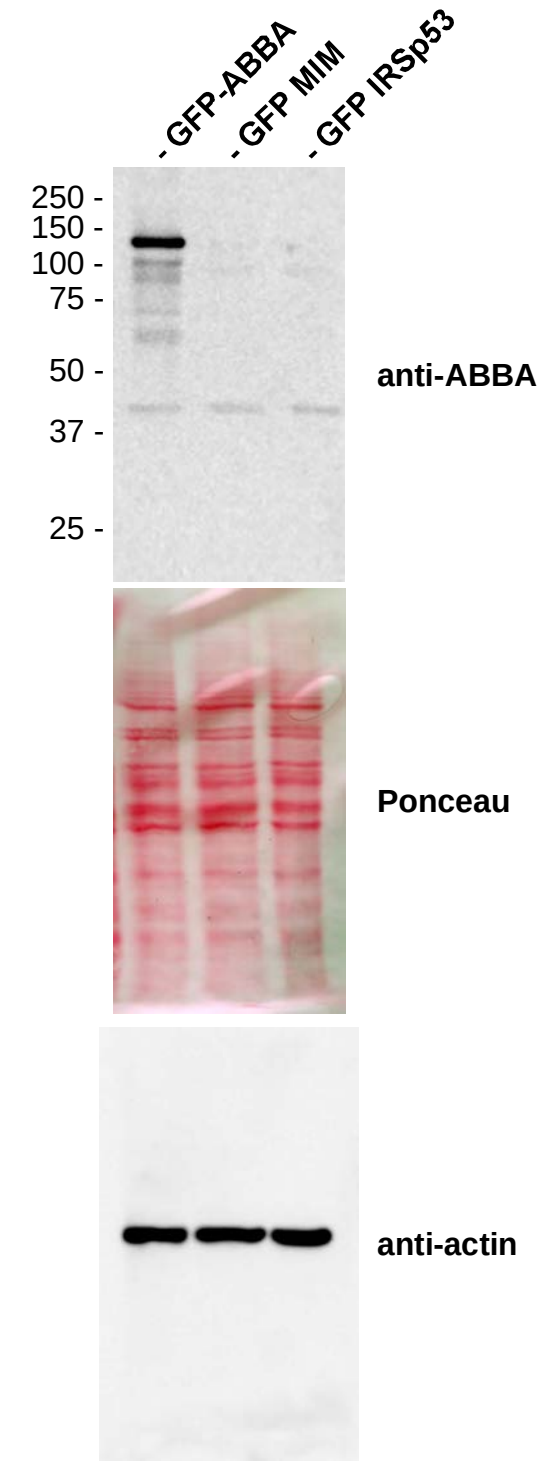
-GFP-ABBA
-GFP MIM
-GFP IRSp53
250 -
150 -
100 -
75 -
50 -
37 -
25 -
anti-ABBA
Ponceau
anti-actin

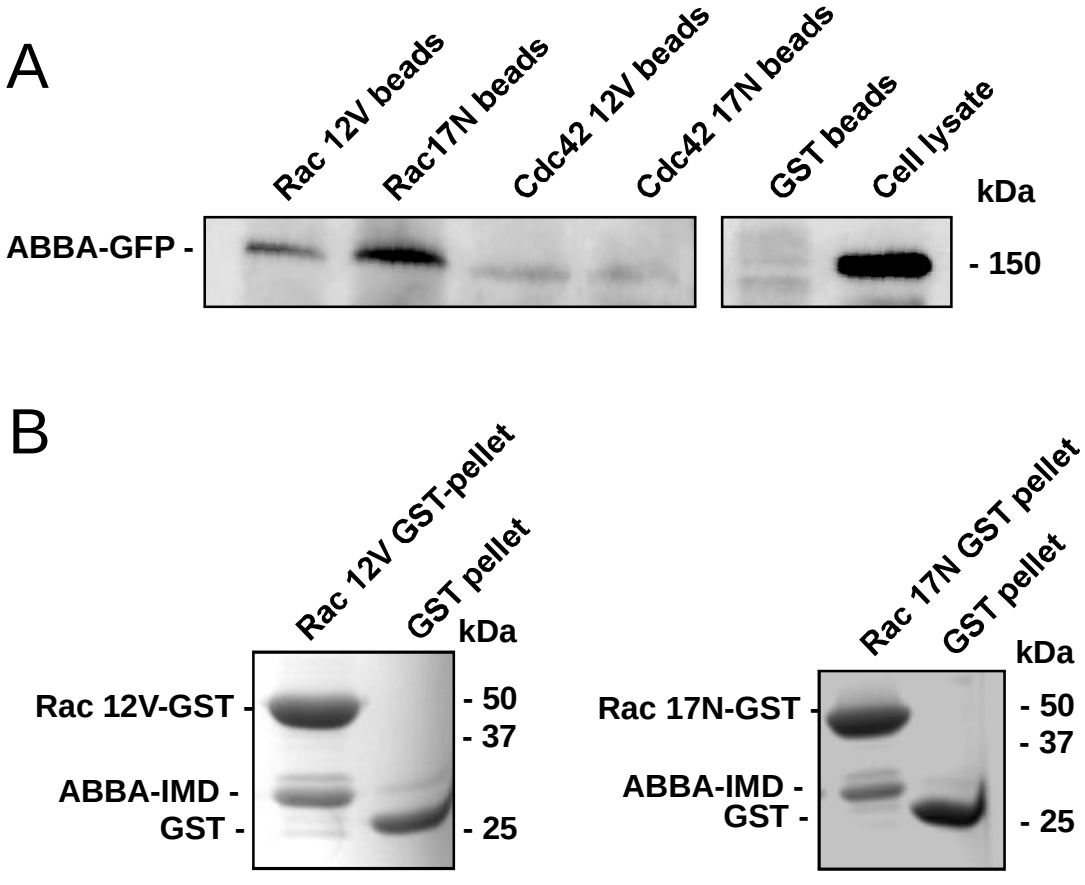
A
Rac 12V beads
Rac17N beads
Cdc42 12V beads
Cdc42 17N beads
GST beads
Cell lysate
kDa
ABBA-GFP -
- 150
B
Rac 12V GST-pellet
GST pellet
kDa
Rac 12V-GST -
ABBA-IMD -
GST -
- 50
- 37
- 25
Rac 17N GST pellet
GST pellet
kDa
Rac 17N-GST -
ABBA-IMD -
GST -
- 50
- 37
- 25

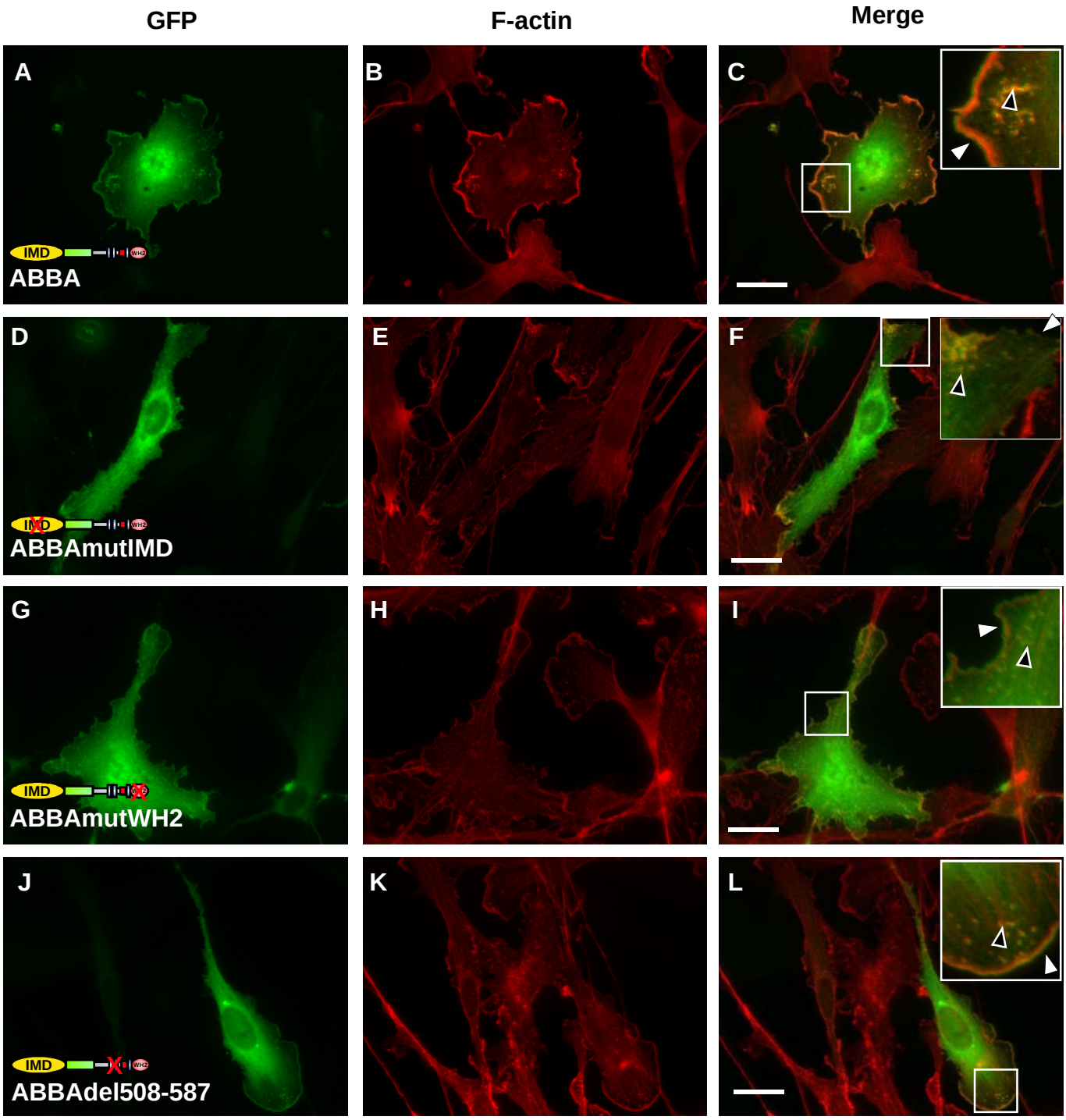
GFP
F-actin
Merge
A
B
C
IMD
WH2
ABBA
D
E
F
IMD
WH2
ABBAmutIMD
G
H
I
IMD
WH2
ABBAmutWH2
J
K
L
IMD
WH2
ABBAdel508-587

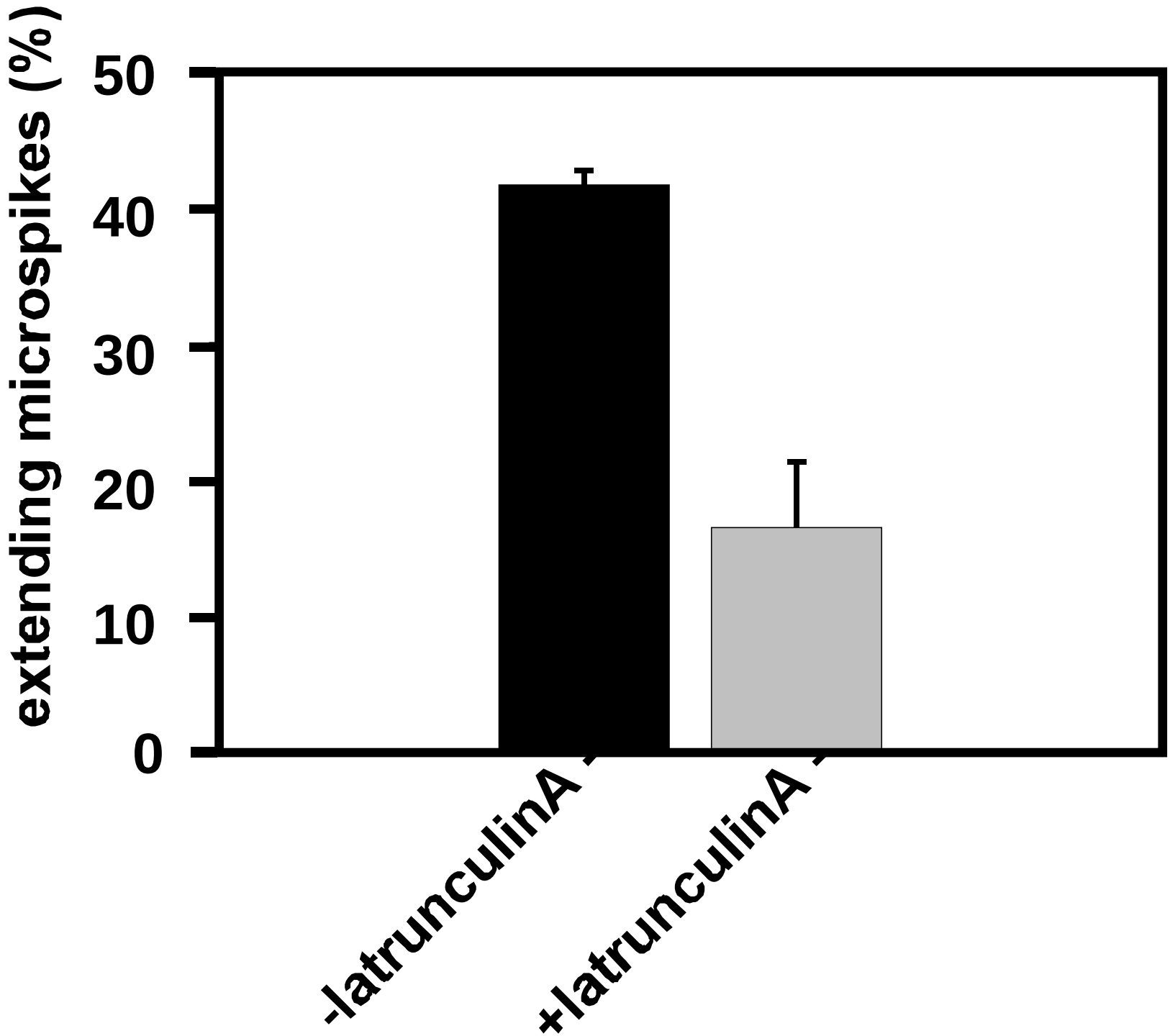
extending microspikes (%)
50
40
30
20
10
0
-latrunculinA
+latrunculinA

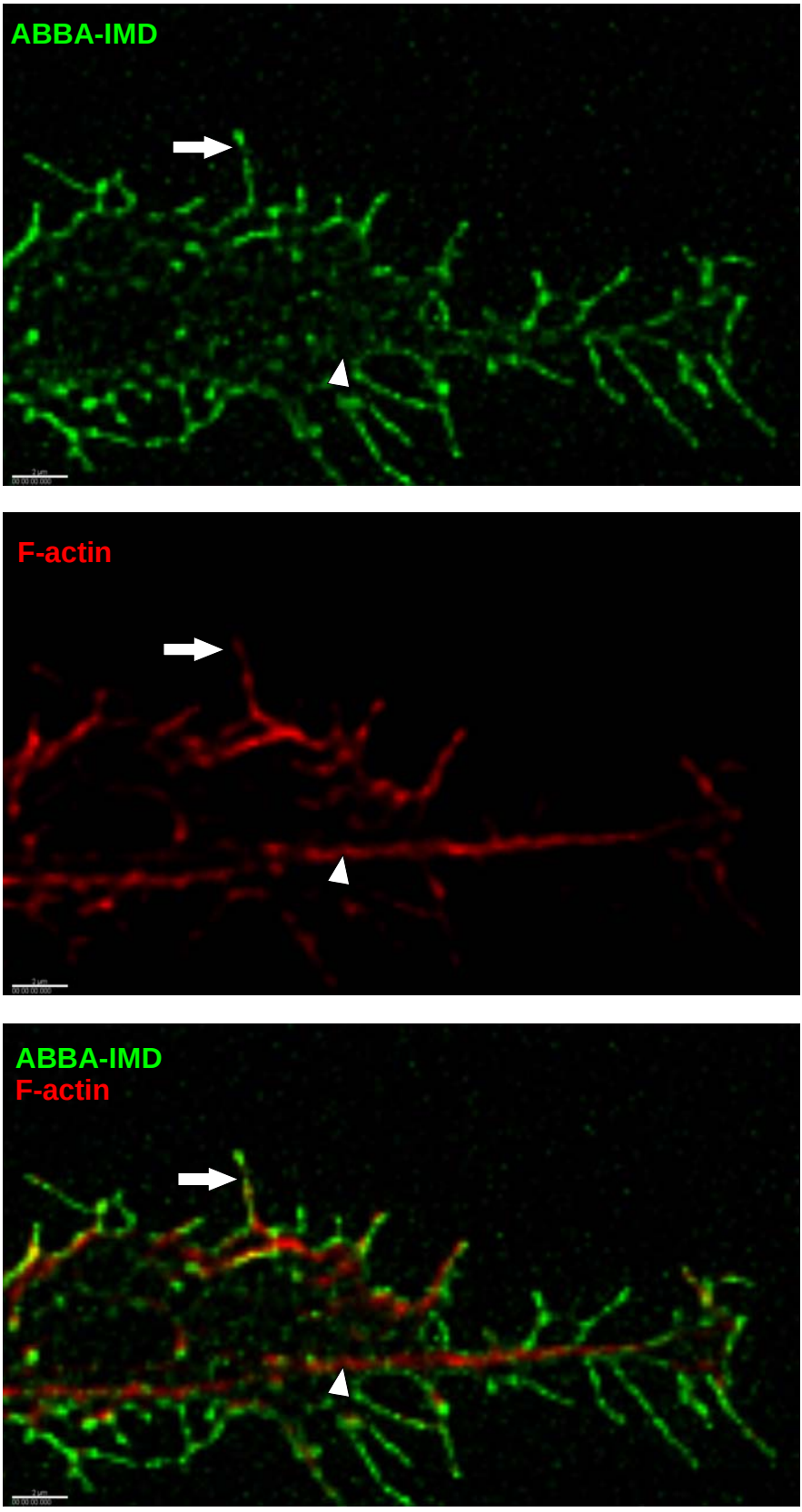
ABBA-IMD
F-actin
ABBA-IMD
F-actin